THE JOURNAL OF PHYSICAL CHEMISTRY C

Article

pubs.acs.org/JPCC

Interfacial Properties of Monolayer $MoSe_2$–Metal Contacts

Yuanyuan Pan,[†,○] Sibai Li,[†,§,○] Meng Ye,[†] Ruge Quhe,[†,∥] Zhigang Song,[†,⊥] Yangyang Wang,[†] Jiaxin Zheng,[§] Feng Pan,[§] Wanlin Guo,[#] Jinbo Yang,[†,‡] and Jing Lu*[,†,‡]

[†]State Key Laboratory for Mesoscopic Physics and Department of Physics, Peking University, Beijing 100871, China

[‡]Collaborative Innovation Center of Quantum Matter, Beijing 100871, China

[§]School of Advanced Materials, Peking University Shenzhen Graduate School, Shenzhen 518055, China

[∥]State Key Laboratory of Information Photonics and Optical Communications, Beijing University of Posts and Telecommunications & School of Science, Beijing 100876, China

[⊥]Department of Nuclear Science and Engineering and Department of Materials Science and Engineering, Massachusetts Institute of Technology, Cambridge, Massachusetts 02139, United States

[#]Key Laboratory for Intelligent Nano Materials and Devices of the Ministry of Education, Beijing 100871, China

ABSTRACT: Monolayer (ML) transition-metal dichalcogenides are considered as promising channel materials in next-generation transistors. Using *ab initio* energy band calculations and more reliable *ab initio* quantum transport simulations, we study the interfacial properties of ML $MoSe_2$–metal interfaces (metals = Al, Ag, Pt, Cr, Ni, and Ti). Weak or medium adsorption is found between ML $MoSe_2$ and the Al, Ag, and Pt surfaces with the band structure of ML $MoSe_2$ preserved, while strong adsorption is found between ML $MoSe_2$ and the Ni, Ti, and Cr surfaces with the band structure of ML $MoSe_2$ destroyed. The two methods give similar polarity and height of Schottky barriers for ML $MoSe_2$ with Al, Ag, Pt, and Ti electrodes. ML $MoSe_2$ forms an *n*-type Schottky contact with Ag, Ti, and Al electrodes with electron Schottky barrier heights (SBH) of 0.25, 0.29, and 0.56 eV, respectively, and a *p*-type Schottky contact with Pt electrode with hole SBH of 0.78 eV according to *ab initio* quantum transport simulations. Our study offers a guidance for the choices of suitable metal electrodes in ML $MoSe_2$ devices.

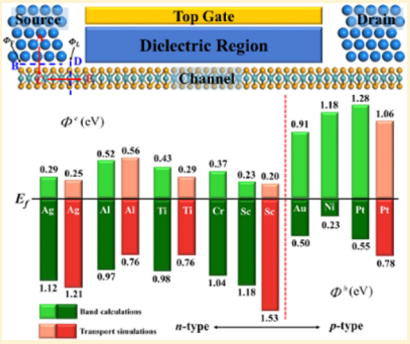

INTRODUCTION

Transition metal dichalcogenides (TMDs) with the formula MX_2 (where M = Mo, W and X = S, Se, and Te) are layered materials characterized by weak interplanar van der Waals coupling and strong in-plane covalent bond.[1,2] High quality few layers or even a single layer large area TMDs have been successfully fabricated with different methods, such as chemical vapor deposition,[3,4] molecular beam epitaxy,[5] and liquid exfoliation[6] *etc.* What is more, the 2D TMDs, with extremely small thickness (a few ångstrom) and the dangling-bond-free surfaces, exhibit a moderate band gap of $E_g \sim 1-2$ eV.[7] A variety of prototype devices based on the 2D TMDs have been constructed or proposed, such as field effect transistors (FETs),[8−12] fully integrated circuits,[13] sensors,[14] spintronic devices,[15] and valleytronic devices.[16−18] Most of the researches of the 2D TMDs are focused on 2D MoS_2 and WSe_2. $MoSe_2$, as a Se counterpart of MoS_2, has a band gap from indirect of 1.1 eV in bulk to direct of 1.5 eV in monolayer (ML).[19,20] Few-layer $MoSe_2$ FETs contacted with Ni and Ti electrodes have been fabricated with a current on/off ratio up to 10^6 and a field-effect motility of 150−200 $cm^2/(V·s)$.[3,9,21,22] Thus, $MoSe_2$ is a promising candidate in electronic applications similar to MoS_2.

Making devices out of 2D TMDs is inevitable to contact with metals. The quality of the electrical contacts is as crucial to the performance of the device as the semiconductor itself.[23,24] Because a finite Schottky barrier usually appears in such electrical contacts, the carrier injection efficiency will decrease. Obviously, how to decrease Schottky barrier height (SBH) is one of the most important thing to gain a high performance of a device. However, the SBH does not merely depend on the discrepancy between the intrinsic Fermi level (E_f) of a metal and the intrinsic conduction band minimum (CBM) or valence band maximum (VBM) of the semiconductor owing to the complex Fermi level pinning. Besides, in the absence of a controllable and sustainable substitutional doping scheme, injecting appropriate types of carriers into the respective bands of 2D TMDs has to rely on the work function of contact metals.[25] Understanding the property of 2D TMDs semiconductor metal interfaces is of great importance.

Compared with the substantial theoretical studies of MoS_2 and WSe_2,[25−30] where a lot of metal electrodes (Sc, Ti, Al, Ag, Cu, Au, Ni, Pt, Pd) have been taken into account, those of ML $MoSe_2$–metal contacts are limited, and only Sc and Au electrodes are considered.[31] Apparently, more metal electrodes are worthy of consideration. In the article, we explore the interfacial characterizes of ML $MoSe_2$ both on high work

Received: March 15, 2016
Revised: May 27, 2016
Published: June 6, 2016

DOI: 10.1021/acs.jpcc.6b02696
J. Phys. Chem. C 2016, 120, 13063−13070

Table 1. Calculated Interfacial Properties of ML $MoSe_2$ on the Metal Electrodes[a]

metal	ε (%)	$d_{Se\text{-}M}$ (Å)	E_b (eV)	W_M (eV)	W (eV)	Φ_V(eV)	Φ_L(eV)	Φ_T^e(eV)	Φ_T^h(eV)	E_g^T(eV)
Al	0.83	3.24	0.04	4.15	4.34	0.52[b]	0.00	0.56	0.76	1.32
Ag	0.21	2.74	0.13	4.45	4.42	0.29[b]	0.00	0.25	1.21	1.46
Pt	4.11	2.80	0.29	5.72	5.28	0.55[c]	0.00	1.06	0.78	1.84
Ti	2.24	2.29	0.71	4.40	4.45	0.00	0.43[b]	0.29	0.76	1.05
Ni	1.02	2.23	0.47	5.20	5.17	0.00	0.23[c]	–	–	–
Cr	1.91	2.38	0.77	4.17	4.38	0.00	0.37[b]	–	–	–

[a]The lattice mismatches is ε. The equilibrium distance $d_{Se\text{-}M}$ is the averaged distance between the surface Se atoms and relaxed positions of the topmost metal layer in the direction vertical to the interfaces. E_b is the binding energy. W_M and W are the calculated work functions for the clean metal surface and the metal surface adsorbed by ML $MoSe_2$, respectively. Φ_V (Φ_L) is the vertical (lateral) SBHs obtained from *ab initio* band calculations. Φ_T^e (Φ_T^h) is the electron (hole) SBH obtained from *ab initio* quantum transport simulations. E_g^T is the transport band gap extracted from *ab initio* quantum transport simulations. The work function of ML $MoSe_2$ is 4.70 eV. [b]For electron SBH. [c]For hole SBH.

function metals Ni and Pt and low work function metals Al, Ag, Ti, and Cr for the first time by applying *ab initio* energy band calculations and *ab initio* quantum transport simulations. It is found that ML $MoSe_2$ forms weak or medium adsorption with the Al, Ag, and Pt electrodes with the band structure of ML $MoSe_2$ preserved and strong adsorption with Ni, Ti, and Cr electrode with the band structure of ML $MoSe_2$ destroyed. In consideration of the more precise *ab initio* quantum transport simulations, *n*-type Schottky contact come into being between ML $MoSe_2$ and the Ag, Ti, and Al electrodes with SBH of 0.25, 0.29, and 0.56 eV, respectively, and *p*-type Schottky contact is formed between ML $MoSe_2$ and Pt electrode with SBH of 0.78 eV. Hence, an opportunity is provided to form ML $MoSe_2$ *p*−*n* junctions by different metal contacts on the two ends of ML $MoSe_2$ without resort of additional doping.

METHODOLOGY

We use five layers of metal atoms to simulate the metal surface and built a supercell with ML $MoSe_2$ adsorbed on the metal surface. Five-layer metal atoms to model the metal surfaces can give converged properties of the contact system in terms of the convergence tests done in the previous studies.[25,27,29,32] Al, Ag, Ni, and Pt in (111) orientation, Ti in (0001) orientation, and Cr in (001) orientation are chosen because they have a high stability and commonly used; especially, the former five orientations correspond to the close-packed face.[26,27,33,34] The in-plane lattice parameter of ML $MoSe_2$ is a = 3.33 Å, which is in good agreement with the experimental value.[35] The ML $MoSe_2$ $\sqrt{3} \times \sqrt{3}$ unit cell is adjusted to the 2 × 2 unit cells of Al, Ag, Pt, and Ti, the ML $MoSe_2$ 2 × 2 unit cell is adjusted to the $2\sqrt{2} \times 2\sqrt{2}$ unit cells of Ni, and the ML $MoSe_2$ $\sqrt{3} \times 2\sqrt{2}$ unit cell is adjusted to the $2 \times 2\sqrt{2}$ unit cells of Cr. The matches are reasonable with all mismatches of smaller than 4.2% (see Table 1). To prevent spurious interaction between periodic images, a vacuum buffer space is set with the value of at least 15 Å. ML $MoSe_2$ mainly interacts with the topmost two layers metal atoms, so the bottom three layers of metal atoms are fixed.

We use plane wave basis set and projector augmented wave (PAW) method[36] implemented in the Vienna *ab initio* simulation package (VASP) code to optimize the structures. The generalized gradient approximation (GGA) functional[37] to the exchange-correction functional of Perdew−Wang 91 (PW91)[38] form is adopted. The plane-wave cut off energy is set to 450 eV to ensure the accuracy. The Brillouin zone are sampled by 3 × 3 × 1 special *k*-points for optimizing these structures and 25 × 25 × 1 to get the densities of states (DOS) using the Monkhorst−Pack scheme.[39] The calculation will not finish until the force is less than 0.01 eV/Å on each atom and the energy between two successive steps is less than 10^{-5} eV.

A gated two-probe model is established to simulate a FET with the most stable ML $MoSe_2$−metal interfaces as the electrodes and the pure ML $MoSe_2$ as the channel. Transport properties of the FET are calculated by using DFT coupled with nonequilibrium Green's function (NEGF) method, as implemented in the ATK 11.8 package.[40−42] We utilize the single-ζ plus polarization (SZP) basis set in the device simulations. GGA of PBE form to the exchange-correlation functional is used through the device simulations. The Monkhorst−Pack *k*-point meshes[39] for electrodes and the central region are sampled with 50 × 50 × 1 and 1 × 50 × 1, separately. The temperature is set to 300 K, and the real-space mesh cutoff is at 75 hartree. We use the Neumann condition on the boundaries of the direction vertical to the ML $MoSe_2$ plane. On the surfaces connecting the electrodes and the central region, Dirichlet boundary condition is employed to ensure the charge neutrality in the source and the drain region. The transmission coefficient $T^{k_{//}}(E)$ ($k_{//}$ is a reciprocal lattice vector point along a surface-parallel direction (orthogonal to the transmission direction) in the irreducible Brillouin zone (IBZ)) is calculated as

$$T^{k_\parallel}(E) = Tr[\Gamma_L^{k_\parallel}(E) G^{k_\parallel}(E) \Gamma_R^{k_\parallel}(E) G^{k_\parallel\dagger}(E)] \quad (1)$$

where, $G^{k_\parallel}$ is the retarded (advanced) Green's function and $\Gamma_{L/R}^{k_\parallel}(E) = i(\sum_{L/R}^{r,k_\parallel} - \sum_{L/R}^{a,k_\parallel})$ presents the level broadening due to left electrode and right electrodes expressed in reference to the electrode self-energies $\sum_{L/R}^{k_\parallel}$, which reflects the effect of electrodes on the scattering region.[31] The transmission function at a given energy $T(E)$ is averaged over different $k_\parallel$ in the IBZ.

RESULTS AND DISCUSSIONS

Geometry and Stability of ML $MoSe_2$−Metal Interfaces. We consider three high-symmetry initial configurations of ML $MoSe_2$ on the Al, Ag, and Pt (111) surfaces. In general, a high-symmetry configuration is more stable than a low-symmetry one and often selected as initial configuration in an actual simulation. In the first initial configuration, the Se atoms sit above the fcc (center of the triangle formed by three neighboring metal surface atoms and having no atom right beneath in the subsurface layer), hcp (center of the triangle formed by three neighboring metal surface atoms and having an atom right beneath in the subsurface layer), and top (right on the top of a metal surface atom) surface sites, and the Mo atoms sit above the centers of the triangle formed by the fcc, hcp, and top surface sites. In the second initial configuration, the Mo atoms sit above the fcc, hcp and top surface sites, and

DOI: 10.1021/acs.jpcc.6b02696
J. Phys. Chem. C 2016, 120, 13063−13070

the Se atoms are above the centers of the triangles formed by the fcc, hcp, and top surface sites. In the third initial configuration, the Mo and Se atoms are all above the centers of the triangles formed by the fcc, hcp, and top surface sites. The most stable configuration of the ML $MoSe_2$−Ag interface comes from the first initial configuration and is shown in Figure 1b. The most stable configuration of the ML $MoSe_2$−Al and −Pt interfaces come from the second initial configuration and are shown in Figure 1(c).

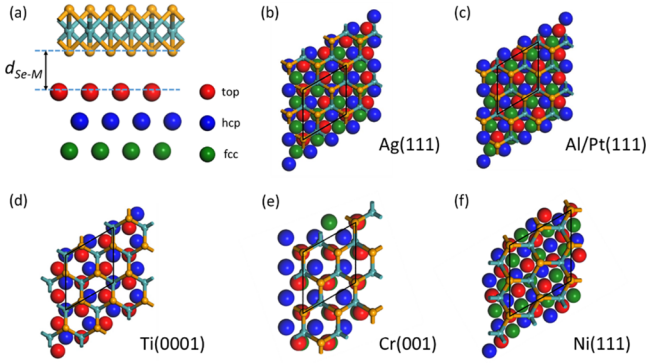

Figure 1. Interfacial structures of the most stable configuration of ML $MoSe_2$ on the metal surfaces. (a) Side views of ML $MoSe_2$ on the metal surfaces. (b) Top view of ML $MoSe_2$ on the Ag(111) surface. (c) Top views of $MoSe_2$ on the Al/Pt(111) surfaces. (d) Top view of ML $MoSe_2$ on the Ti(0001) surface. (e) Top views of $MoSe_2$ on the Cr(001) surface. (f) Top views of $MoSe_2$ on the Ni(111) surface. The rhombi plotted in black line shows the unit cell for each structure. The yellow and light blue balls present Se and Mo atoms, respectively.

We adopt two initial configurations of ML $MoSe_2$−Ti (0001), Cr (001), and Ni (111) surfaces. For ML $MoSe_2$ on the Ti (0001) surface: the first is that the Mo atoms site above the top metal atoms and the Se atoms site above the centers of triangles, while the second is that the Se atoms site above the top metal atoms and the Mo atoms site above centers of triangles. The most stable configuration of ML $MoSe_2$−Ti interface is shown in Figure 1(d), which comes from the first initial configuration. For ML $MoSe_2$ on the Cr (001) surface: One is that the four vertex Mo atoms in the supercell site above the top metal atoms, and the other is the four vertex Se atoms in the supercell site above the top metal atoms. The most stable configuration of ML $MoSe_2$−Cr interface is shown in Figure 1e, which originates from the first initial one. For ML $MoSe_2$ on the Ni (111) surface: One is that the four vertex Mo atoms in the supercell site above the top metal atoms, while the other is one of the Mo atom inside the rhombus sites above the top metal atoms. The most stable configuration of ML $MoSe_2$−Cr interface is shown in Figure 1f, which comes from the first initial configuration.

Table 1 is the summary of the calculated key results of ML $MoSe_2$−metal interfaces studied in this work. The equilibrium interfacial distances $d_{Se\text{-}M}$ is defined as the difference between the average z-coordinates (vertical to the interface) of the bottom layer Se atoms and the topmost layer metal atoms (Figure 1a). It varies from 2.29−3.24 Å, decreasing in the order of Al > Pt > Ag > Cr > Ti > Ni. The binding energy per interfacial Se atom is defined as

$$E_b = (E_{MoSe_2} + E_{metal} - E_{MoSe_2-metal})/N_{Se} \quad (2)$$

where E_{MoSe_2}, E_{metal}, $E_{MoSe_2-metal}$ are the relaxed energies for ML $MoSe_2$, the metal surface, and the ML $MoSe_2$−metal system, respectively, and N_{Se} is the number of interface Se atoms in a supercell. In view of $d_{Se\text{-}M}$ and E_b, three types of adsorption of ML $MoSe_2$−metal interfaces are classified. Al and Ag have weak adsorption and large interfacial distances with ML $MoSe_2$ (E_b = 0.04−0.13 eV and $d_{Se\text{-}M}$ = 2.74−3.24 Å), and Pt has a medium adsorption and interfacial distance with ML $MoSe_2$ (E_b = 0.29 eV and $d_{Se\text{-}M}$ = 2.80 Å), and Ni, Ti, and Cr have a strong adsorption and a small distance with ML $MoSe_2$ (E_b = 0.47−0.77 eV and $d_{Se\text{-}M}$ = 2.23−2.38 Å).

Electronic Structure of ML $MoSe_2$−Metal Interfaces. The band structures of the interfacial systems and pure ML $MoSe_2$ are shown in Figure 2. The direct band gap of the pure

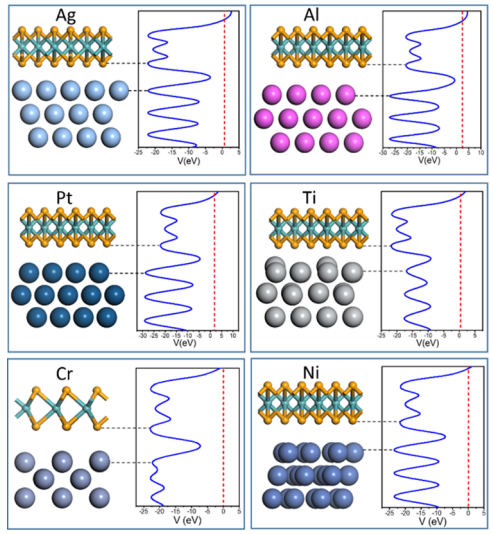

Figure 2. Side view of the optimized structures and average effective potentials in planes normal to the interface of ML $MoSe_2$ systems with Al, Ag, Pt, Ti, Cr, and Ni, respectively. The Fermi level is set to zero.

ML $MoSe_2$ is 1.41 eV, which is consistent with the previous density functional theory (DFT) value of 1.44 eV.[43] The hybridization degrees of the band structures for ML $MoSe_2$ adsorbed on metals are different. When contacted with Ni, Ti, and Cr, both the conduction and the valence bands of ML $MoSe_2$ are seriously destroyed, suggestive of a strong band hybridization (mixtures of the bands of the interfacial metal atoms and those of the interfacial Se atoms). Though the valence bands of ML $MoSe_2$ are destroyed weakly, the conduction band is still reserved well (suggestive of a moderate hybridization), when contacted with Pt. The band of ML $MoSe_2$ is still discernible (suggestive of a slight hybridization) when contacted with Ag and Al. The different hybridization degrees result from the different occupied level and radius of d-orbital of metals. Pt, Ni, Ti, and Cr have partially occupied d-orbitals, which form covalent bond with the 4p orbitals of the interfacial Se atoms and lead to a larger binding energy (E_b = 0.29−0.77 eV). Pt has a larger d-orbital radius than Ti, Ni, and Cr and therefore has a weaker hybridization degree and a weaker adsorption than Ti, Ni, and Cr. Al has unfilled d-orbitals and Ag has fully filled d-orbital, and thus the d-orbitals of Ag and Al hardly form covalent bond with the orbitals of the interfacial Se atoms, causing a preservation of the band structure of $MoSe_2$ and a smaller binding energy with $MoSe_2$ (E_b = 0.04 and 0.13 eV for Al and Ag, respectively). The weaker

DOI: 10.1021/acs.jpcc.6b02696
J. Phys. Chem. C 2016, 120, 13063−13070

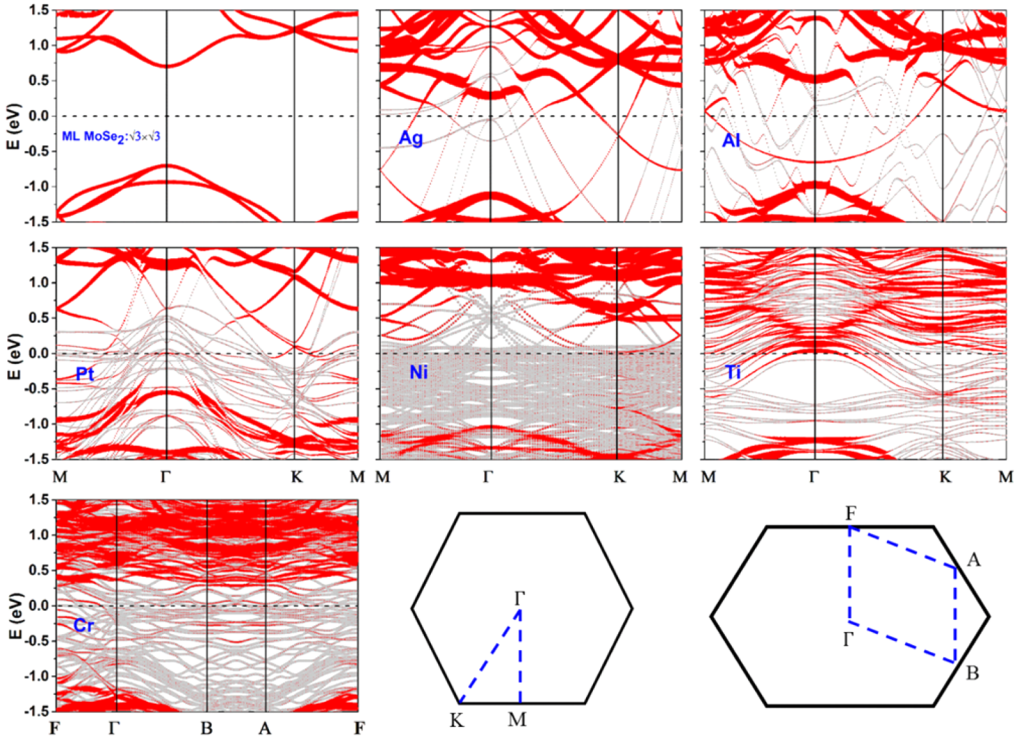

Figure 3. Band structures of pure $MoSe_2$ ($\sqrt{3} \times \sqrt{3}$) and ML $MoSe_2$−Al, −Ag, −Pt, −Ni, −Cr, and −Ti contacts, respectively. Gray line: band structures of ML $MoSe_2$−metal systems; red line: band structures of ML $MoSe_2$. The line width is proportional to the weight. The Fermi level is at zero energy. Diagram of the bottom right: the two-dimensional Brillouin zone of ML $MoSe_2$ for the $\sqrt{3} \times \sqrt{3}$ and the $\sqrt{3} \times 2\sqrt{2}$ unit cells.

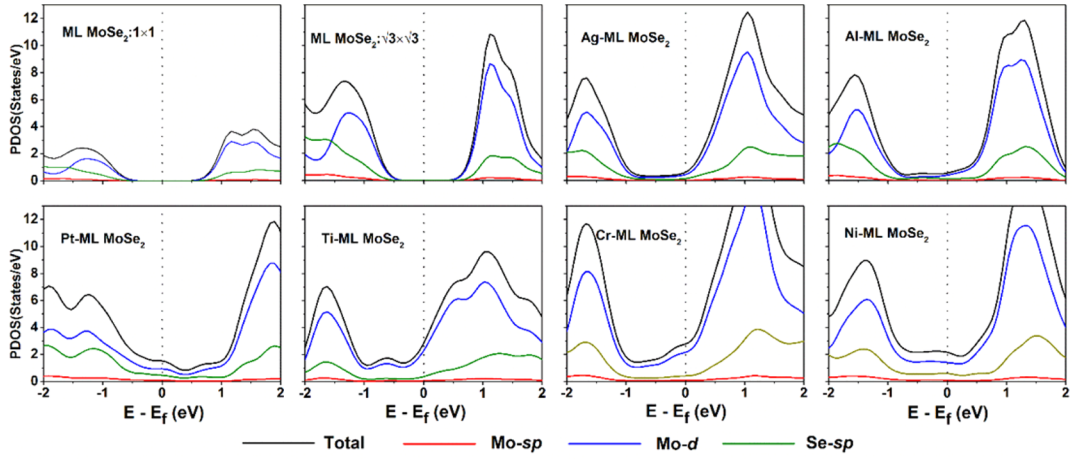

Figure 4. Partial density of states (PDOS) (DOS on specified atoms and orbitals, for example, Mo-d (d-orbital on Mo) of $MoSe_2$ on the Al, Ag, Pt, Ti, Cr, and Ni surfaces at the DFT level. The Fermi level is at zero energy. The PDOS of free-standing $MoSe_2$ calculated in a primitive unit cell and a $\sqrt{3} \times \sqrt{3}$ supercell is provided for comparison.

adhesion of Al to $MoSe_2$ is ascribed to a lower doping (charge transfer between metals and ML $MoSe_2$) level of Al to $MoSe_2$ than Ag to $MoSe_2$, which is apparent from a smaller deviation of E_f to the band gap center in Al (0.24 eV) than Ag (0.40 eV).

To deeply understand the hybridization degree of the band structures for ML $MoSe_2$ adsorbed on metals, we calculate the partial density of states (PDOS) on Se and Mo orbitals of ML $MoSe_2$−metal systems as shown in Figure 4. It is mainly the Mo *d* and Se *sp* states that arise in the pristine band gap of ML $MoSe_2$, while the Mo *sp* states are invariable after ML $MoSe_2$ adsorbed on the investigated metals. In slight hybridization (ML $MoSe_2$−Al and -Ag interfaces), only a small portion of Mo and Se states distribute in the pristine band gap of ML $MoSe_2$ and the valence and conduction bands can be identified, thus ML $MoSe_2$ still preserves most semiconducting natures. In moderate and strong hybridization (ML $MoSe_2$−Pt, Ni, Ti, and Cr interfaces), a large portion of Mo and Se states arise in the original band gap of ML $MoSe_2$. The PDOS at E_f decreases in the order: Cr > Ti > Ni > Pt > Ag > Al, which is consistent with the band structure hybridization degree. Together with the fact that a large amount of bands of ML $MoSe_2$ appear at the original band gap of free-standing ML $MoSe_2$ in the ML $MoSe_2$−Ti, Ni, and Cr systems (Figure 3.), we can identify a metallization for ML $MoSe_2$ at these surfaces.

The schematic drawing of a ML $MoSe_2$ FET is shown in Figure 8a. The most reasonable interfacial model to describe

DOI: 10.1021/acs.jpcc.6b02696
J. Phys. Chem. C 2016, 120, 13063−13070

the 2D FET's Schottky barriers is dual-interfaces model in our opinion, which has been extensively adopted in the previous studies.[25,27,44] According to the dual-interfaces model, Schottky barriers can arise at either of the two distinct interfaces in ML $MoSe_2$ FETs: One is between the contacted metal and the below ML $MoSe_2$ in the vertical direction if the adsorption between the 2D material and metals is weak or medium (labeled interface B, and the corresponding SBH is labeled Φ_V), and the other is between the strongly contacted systems and the channel ML $MoSe_2$ in the lateral direction if the contacted 2D semiconductor undergoes a metallization as a result of strong interaction with metal (labeled interface D, and the corresponding SBH is labeled Φ_L). Besides, tunneling barrier can come out at interface B when electrons traverse the gap (normally van der Waals gap) between ML $MoSe_2$ and metals.

For ML MoSe2 on the Al, Ag, and Pt electrodes, the adhesion is weak or medium, and therefore the Schottky barriers appear in the vertical direction. Vertical SBHs Φ_V can be extracted from the energy band structure (depicted in Figure 3) by comparing the Fermi level and the identifiable band edges of ML $MoSe_2$ in the interfacial system. The extracted electron SBHs Φ_V^e of Ag and Al electrodes are 0.29 and 0.52 eV, respectively, while the hole SBH Φ_V^h of Pt electrode is 0.55 eV. The vertical SBH of Ti, Ni, and Cr electrodes vanish owing to the band hybridizations between ML $MoSe_2$ and Ni, Ti, and Cr electrodes, which leads to a metallization of ML $MoSe_2$ under metals.

For ML $MoSe_2$ on Ti, Ni, and Cr electrode, the adhesion is strong, and thus the Schottky barriers appear in the lateral direction. The energy differences from the interfacial system E_f to the CBM (VBM) of freestanding channel ML $MoSe_2$ determine the lateral electron SBHs Φ_L^e (hole SBHs Φ_L^h) in the energy band scheme.[44,45] According to such a scheme, the lateral hole SBH Φ_L^h of Ni electrode is 0.23 eV, and the electron SBHs Φ_L^e of Cr and Ti are 0.37 and 0.43 eV, respectively. The tunneling barrier ΔV is defined as the potential energy above E_f at the interfaces between ML $MoSe_2$ and the metal. The potential profiles at the vertical ML $MoSe_2$–metal interfaces are shown in Figure 2. No tunneling barriers appear at all the ML $MoSe_2$–metal interfaces because the potentials at interface are below the Fermi level.

Quantum Transport Simulations and Comparison of the Schottky Barriers. To further clarify the contact properties of the real ML $MoSe_2$ FET, ML $MoSe_2$ FETs with Ag, Al, Ti, and Pt electrodes are simulated. The transmission spectra of those ML $MoSe_2$ FETs with the channel length L = 5 nm at zero bias are depicted in Figure 5. According our experiences in previous work,[46] a 5 nm channel is enough to present SBHs of 2D semiconductor transistors. What's more, the transport gap of 5 nm channel ML $MoSe_2$ is consistent with the band gap of pure ML $MoSe_2$. The electron (hole) SBHs are extracted by the divergence between the Fermi level and the CBM (VBM) in the zero transmission spectra. ML $MoSe_2$ forms *n*-type Schottky contact with Ag, Ti, and Al electrodes with electron SBH of 0.25, 0.29, and 0.56 eV, respectively, while forms *p*-type Schottky contact with Pt electrode with hole SBH of 0.78 eV. The transport gap is a sum of electron and hole SBH: $E_g^T = \Phi_T^e + \Phi_T^h$, and the transport gap E_g^T for Ti, Al, Ag, and Pt electrodes is 1.05, 1.32, 1.46, and 1.84 eV, respectively, contrasted with a band gap of 1.41 eV for pristine ML $MoSe_2$ in the energy band calculation.

Local device density of state (LDDOS) is visualization of the energy band in real space. We calculate the LDDOS in ML

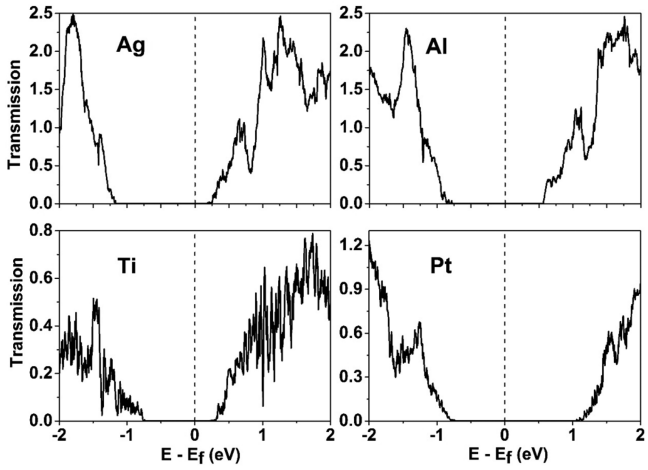

Figure 5. Zero-bias transmission spectra of ML $MoSe_2$ FETS with Ag, Al, Ti, and Pt electrodes. The channel length is 5 nm.

$MoSe_2$ FETs with Ag, Al, Ti, and Pt electrodes, as shown in Figure 6. The SBHs in ML $MoSe_2$ FETs extracted from the

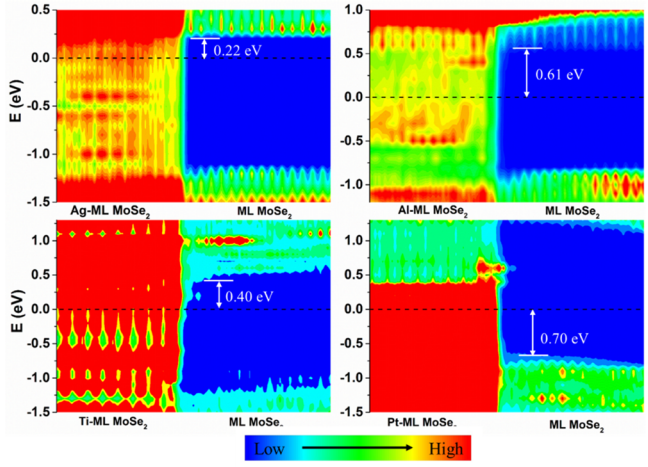

Figure 6. LDDOS in color coding for ML $MoSe_2$ FETs of channel length L = 5 nm with Ag, Al, Ti, and Pt electrodes, respectively. The Fermi level is at zero energy. The SBHs are indicated and determined from the difference between E_f and the CBM or VBM.

LDDOS are similar to those calculated in transmission spectra. ML $MoSe_2$ with Ag, Ti, and Al electrodes are *n*-type Schottky FETs with SBHs of 0.22, 0.40, and 0.61 eV, respectively, compared with the respective values of 0.25, 0.29, and 0.56 eV obtained from the transmission spectra. ML $MoSe_2$ with Pt electrode is *p*-type Schottky FET with SBH of 0.70 eV, alike to the value of 0.78 eV obtained from the transmission spectra.

A vital nature in a metal–semiconductor interfaces is band bending away from the contact. For ML $MoSe_2$ contacting with Ag electrode, the conduction band is slightly bent upward due to electrons divert from electrodes to channel ML $MoSe_2$. For ML $MoSe_2$ contacting with Al and Ti electrodes, the conduction bands are apparently bent upward because of electrons divert from electrodes to channel ML $MoSe_2$ forming a *n*-type contact. For $MoSe_2$ contacting with Pt, the valence band is bend down, because an inverse electrons divert from electrodes to channel ML $MoSe_2$ forming a *p*-type contact, as shown in Figure 6.

DOI: 10.1021/acs.jpcc.6b02696
J. Phys. Chem. C 2016, 120, 13063–13070

The metal−semiconductor coupling in a FET takes place either at the interface B between metal electrodes and the below 2D semiconductor or at the interface D between the metallized electrodes and channel semiconductor. Both the two couplings are taken into account in *ab initio* quantum transport simulations because the FET is treated as a whole, while only the coupling at the interface B is considered in *ab initio* energy band calculations scheme. The metal−semiconductor coupling at the interface D is not considered in *ab initio* energy band calculations scheme that requires a periodical condition because the metallized part and the channel semiconductor part are treated separately. Therefore, *ab initio* quantum transport simulations are expected to give more dependable SBH at the interface D, while *ab initio* energy band calculations are less reliable due to the ignorance of the metal−semiconductor coupling at the interface D.[26,27,46] In other word, for a 2D transistor with a strong adhesion between metal electrode and underlying 2D semiconductors, which implies that the Schottky barrier appear at the interface D, *ab initio* quantum transport simulations are more reliable than *ab initio* energy band calculations in predicting the SBH.

The reliability of *ab initio* quantum transport simulation against *ab initio* energy band calculations in predicting the SBH of a 2D transistor with a strong adhesion between metal electrode and underlying 2D semiconductors has been verified in ML phosphorene transistor with Ni electrode, in which the hole SBH of ML phosphorene FET in the transport simulation (0.26 eV) is much larger than that in the energy band analysis (0.02 eV) with Ni electrode.[46] The experimental transport hole SBH of ML phosphorene is 0.35 ± 0.02 eV with Ni electrode,[47] preferring the *ab initio* quantum transport simulation result. Another evidence is in 2D MoS_2 transistor with Sc electrode, in which for 2D MoS_2−Sc contact, a pseudo Ohmic contact appears according to energy band analysis and an electron SBH of 0.15 eV is calculated in quantum transport simulation. The latter is qualitatively consistent with the experiment electron SBH of 0.03 eV.[26,48]

Moreover, the carrier polarity of the Schottky barriers is even different in the two methods. For example, when Cr, Au, Cu, and Ti are used as electrodes, the carrier polarity of ML phosphorene FET is entirely opposite in the two methods.[46] For Cr, Au, and Cu as electrodes, *p*-type Schottky one in the electronic band structure calculations changes into *n*-type Schottky one in the quantum transport simulations in ML phosphorene FETs. Otherwise, for Ti as electrode, ML phosphorene FET changes from *n*-type Schottky contact with a larger hole SBH of 0.51 eV in the energy band analysis to *p*-type Schottky contact with a smaller hole SBH of 0.30 eV in the quantum transport simulations. The reported experiments support the quantum transport simulation results and show that *p*-type Schottky phosphorene FET is formed with Ti electrode, and few layers phosphorene has a hole SBH of 0.21 eV with Ti electrode.[49]

A comparison of the SBHs of ML $MoSe_2$ on those metal electrodes between *ab initio* energy band calculations and *ab initio* quantum transport simulations is depicted in Figure 7. The polarity and size of the SBHs of the Schottky contacts for ML $MoSe_2$ with Ag, Al, Ti, and Pt electrodes obtained in the two methods resemble one another. The consistency between the two methods for ML $MoSe_2$ with Ag, Al, and Pt electrodes are not unexpected because the Schottky barrier appears at interface B, and in this case both methods have taken into consideration the interaction between metal and semiconductor. The similar polarity and size of the SBHs for ML $MoSe_2$ with Ti electrode in the two methods is somewhat unexpected and indicates a weak coupling between Ti electrode and the channel ML $MoSe_2$ without significant Fermi level pinning. The similar polarity and size of the SBHs for ML $MoSe_2$ with Sc electrode (strong adhesion) are also calculated in the two methods in the previous work[31] and indicates a weak coupling between Sc electrode and the channel ML $MoSe_2$ without significant Fermi level pinning. For the sake of comparison, we provide the SBHs of Sc and Au electrodes calculated in the previous work[31] in Figure 7, and from this figure, the Sc electrode has the smallest SBH (0.20−0.23 eV) in all checked electrodes.[48]

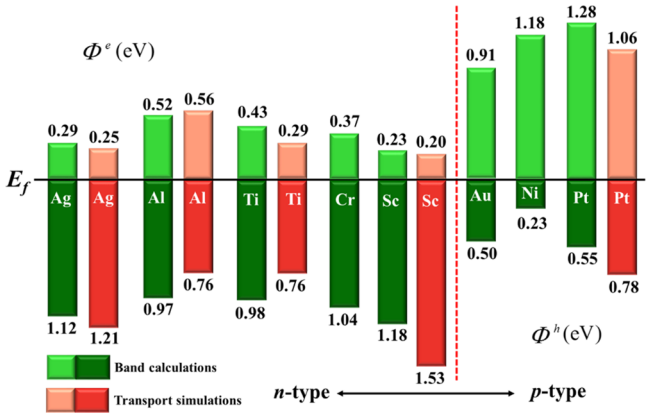

Figure 7. Comparison of the SBH (Φ^e for electron and Φ^h for hole) of ML $MoSe_2$ on Ag, Al, Ti, Cr, Sc, Au, Ni, and Pt electrodes, respectively, obtained by the *ab initio* electronic band calculations and *ab initio* quantum transport calculations. The SBHs of Sc and Au are from ref 31

In view of tunneling barriers and Schottky barriers, four kinds of ML $MoSe_2$−metal contact are identified, as shown in Figure 8b−e. ML $MoSe_2$ forms the type I (II) contact with Ti and Cr (Ni) electrode, in which electrons (hole) directly inject from A region to C region without barriers at the interface B and

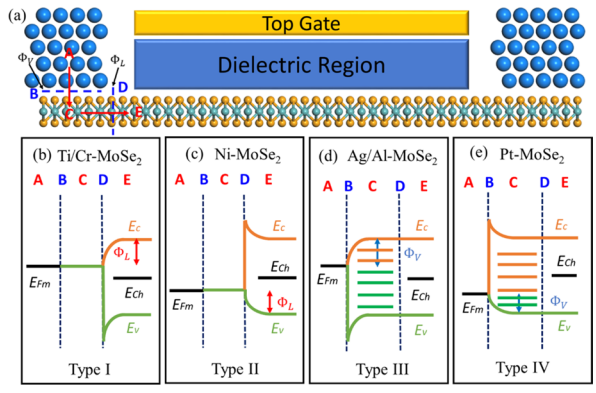

Figure 8. (a) Schematic diagram of a ML $MoSe_2$ FET. Schematic cross-sectional view of a typical metal contact to intrinsic ML $MoSe_2$ channel. A, C, and E denotes three regions, while B and D are the two interfaces separating them. Red rows show the pathway (A → B → C → D → E) of electron or hole injection from contact metal (A) to the ML $MoSe_2$ channel (E). (b−e) Four possible band diagrams of the ML $MoSe_2$ FETs in view of Schottky barriers and tunneling barrier, depending on the type of metal. Examples are provided at the bottom of each diagram. E_{Fm} and E_{Ch} denote the Fermi level of the interfacial systems and channel ML $MoSe_2$, respectively.

DOI: 10.1021/acs.jpcc.6b02696
J. Phys. Chem. C 2016, 120, 13063−13070

encounter a *n*-type (*p*-type) Schottky barrier at the lateral interface D. ML $MoSe_2$ forms the type III (type IV) contact with Al and Ag (Pd), in which electrons (holes) only face a *n*-type (*p*-type) Schottky barrier at the vertical interface B.

CONCLUSIONS

This work presented a theoretical study of the physical nature of ML $MoSe_2$−Al, −Ag, −Pd, −Cr, −Ti, and −Ni interfaces for the first time. Two categories are untangled according to the adsorption level: weak or medium adsorption is found in ML $MoSe_2$ and Al, Ag, and Pd contacts; strong adsorption is found in ML $MoSe_2$ and Ti, Ni, and Cr contacts. We calculate the SBHs by applying both *ab initio* energy band calculations and more dependable *ab initio* quantum transport simulations. For weak adsorption, the two methods give similar type and size of SBH, because SBH is formed in the vertical direction, and both the two methods take into consideration the interaction between metal and ML $MoSe_2$ at the interface B. For strong adsorption with Ti electrode, SBH is formed in the lateral directions, and the two methods luckily give similar type and size SBH and suggest absence of Fermi level pining between Ti electrode and the channel ML $MoSe_2$.

AUTHOR INFORMATION

Corresponding Author

*(J.L.) Telephone: 86-010-62755701. E-mail: jinglu@pku.edu.cn.

Author Contributions

○These authors contributed equally to this work.

Notes

The authors declare no competing financial interest.

ACKNOWLEDGMENTS

This work was supported by the National Natural Science Foundation of China (No. 11274016/11474012), the National Basic Research Program of China (No. 2013CB932604/2012CB619304), the National Science Foundation Grant (1207141), National Foundation for Fostering Talents of Basic Science (No. J1030310/No. J1103205), and Open Fund of Key Laboratory for Intelligent Nano Materials and Devices of the Ministry of Education (INMD-2016M03).

REFERENCES

(1) Wang, Q. H.; Kalantar-Zadeh, K.; Kis, A.; Coleman, J. N.; Strano, M. S. Electronics and Optoelectronics of Two-dimensional Transition Metal Dichalcogenides. *Nat. Nanotechnol.* **2012**, *7*, 699−712.

(2) Chhowalla, M.; Shin, H. S.; Eda, G.; Li, L. J.; Loh, K. P.; Zhang, H. The Chemistry of Two-dimensional Layered Transition Metal Dichalcogenide Nanosheets. *Nat. Chem.* **2013**, *5*, 263−275.

(3) Wang, X.; Gong, Y.; Shi, G.; Chow, W.; Keyshar, K.; Ye, G.; Vajtai, R.; Lou, J.; Liu, Z.; Ringe, E.; et al. Chemical Vapor Deposition Growth of Crystalline Monolayer $MoSe_2$. *ACS Nano* **2014**, *8*, 5125−5131.

(4) Xia, J.; Huang, X.; Liu, L. Z.; Wang, M.; Wang, L.; Huang, B.; Zhu, D. D.; Li, J. J.; Gu, C. Z.; Meng, X. M. CVD Synthesis of Large-area, Highly Crystalline $MoSe_2$ Atomic Layers on Diverse Substrates and Application to Photodetectors. *Nanoscale* **2014**, *6*, 8949−8955.

(5) Jiao, L.; Liu, H. J.; Chen, J. L.; Yi, Y.; Chen, W. G.; Cai, Y.; Wang, J. N.; Dai, X. Q.; Wang, N.; Ho, W. K.; et al. Molecular-beam Epitaxy of Monolayer $MoSe_2$: Growth Characteristics and Domain Boundary Formation. *New J. Phys.* **2015**, *17*, 053023.

(6) Coleman, J. N.; Lotya, M.; O'Neill, A.; Bergin, S. D.; King, P. J.; Khan, U.; Young, K.; Gaucher, A.; De, S.; Smith, R. J.; et al. Two-dimensional Nanosheets Produced by Liquid Exfoliation of Layered Materials. *Science* **2011**, *331*, 568−571.

(7) Coehoorn, R.; Haas, C.; Dijkstra, J.; Flipse, C. J. F.; de Groot, R. A.; Wold, A. Electronic Structure of $MoSe_2$, MoS_2, and WSe_2. I. Band-Structure Calculations and Photoelectron Spectroscopy. *Phys. Rev. B: Condens. Matter Mater. Phys.* **1987**, *35*, 6195−6202.

(8) Radisavljevic, B.; Radenovic, A.; Brivio, J.; Giacometti, V.; Kis, A. Single-layer MoS_2 Transistors. *Nat. Nanotechnol.* **2011**, *6*, 147−150.

(9) Larentis, S.; Fallahazad, B.; Tutuc, E. Field-effect Transistors and Intrinsic Mobility in Ultra-thin MoSe2 Layers. *Appl. Phys. Lett.* **2012**, *101*, 223104.

(10) Baugher, B. W.; Churchill, H. O.; Yang, Y.; Jarillo-Herrero, P. Intrinsic Electronic Transport Properties of High-quality Monolayer and Bilayer MoS_2. *Nano Lett.* **2013**, *13*, 4212−4216.

(11) Sarkar, D.; Liu, W.; Xie, X.; Anselmo, A. C.; Mitragotri, S.; Banerjee, K. MoS_2 Field-Effect Transistor for Next-Generation Label-Free Biosensors. *ACS Nano* **2014**, *8*, 3992−4003.

(12) Das, S. R.; Kwon, J.; Prakash, A.; Delker, C. J.; Das, S.; Janes, D. B. Low-frequency Noise in $MoSe_2$ Field Effect Transistors. *Appl. Phys. Lett.* **2015**, *106*, 083507.

(13) Radisavljevic, B.; Whitwick, M. B.; Kis, A. Integrated Circuits and Logic Operations Based on Single-Layer MoS_2. *ACS Nano* **2011**, *5*, 9934−9938.

(14) Perkins, F. K.; Friedman, A. L.; Cobas, E.; Campbell, P. M.; Jernigan, G. G.; Jonker, B. T. Chemical Vapor Sensing with Monolayer MoS_2. *Nano Lett.* **2013**, *13*, 668−673.

(15) Yuan, H.; Bahramy, M. S.; Morimoto, K.; Wu, S.; Nomura, K.; Yang, B.-J.; Shimotani, H.; Suzuki, R.; Toh, M.; Kloc, C.; et al. Zeeman-type Spin Splitting Controlled by an Electric Field. *Nat. Phys.* **2013**, *9*, 563−569.

(16) Zeng, H.; Dai, J.; Yao, W.; Xiao, D.; Cui, X. Valley Polarization in MoS_2 Monolayers by Optical Pumping. *Nat. Nanotechnol.* **2012**, *7*, 490−493.

(17) Mak, K. F.; He, K.; Shan, J.; Heinz, T. F. Control of Valley Polarization in Monolayer MoS_2 by Optical Helicity. *Nat. Nanotechnol.* **2012**, *7*, 494−498.

(18) Song, Z.; Quhe, R.; Liu, S.; Li, Y.; Feng, J.; Yang, Y.; Lu, J.; Yang, J. Tunable Valley Polarization and Valley Orbital Magnetic Moment Hall Effect in Honeycomb Systems with Broken Inversion Symmetry. *Sci. Rep.* **2015**, *5*, 13906.

(19) Zhang, Y.; Chang, T. R.; Zhou, B.; Cui, Y. T.; Yan, H.; Liu, Z.; Schmitt, F.; Lee, J.; Moore, R.; Chen, Y.; et al. Direct Observation of the Transition from Indirect to Direct Bandgap in Atomically Thin Epitaxial $MoSe_2$. *Nat. Nanotechnol.* **2014**, *9*, 111−115.

(20) Tongay, S.; Zhou, J.; Ataca, C.; Lo, K.; Matthews, T. S.; Li, J.; Grossman, J. C.; Wu, J. Thermally Driven Crossover from Indirect toward Direct Bandgap in 2D Semiconductors: $MoSe_2$ versus MoS_2. *Nano Lett.* **2012**, *12*, 5576−5580.

(21) Pradhan, N. R.; Rhodes, D.; Xin, Y.; Memaran, S.; Bhaskaran, L.; Siddiq, M.; Hill, S.; Ajayan, P. M.; Balicas, L. Ambipolar Molybdenum Diselenide Field-effect Transistors: Field-effect and Hall Mobilities. *ACS Nano* **2014**, *8*, 7923−7929.

(22) Chamlagain, B.; Li, Q.; Ghimire, N. J.; Chuang, H.-J.; Tu, H.; Xu, Y.; Pan, M.; Xaio, D.; Yan, J.; Perera, M. M.; et al. Mobility Improvement and Temperature Dependence in $MoSe_2$ Field-Effect Transistors on Parylene-c Substrate. *ACS Nano* **2014**, *8*, 5079−5088.

(23) Allain, A.; Kang, J.; Banerjee, K.; Kis, A. Electrical Contacts to Two-dimensional Semiconductors. *Nat. Mater.* **2015**, *14*, 1195−1205.

(24) Leonard, F.; Talin, A. A. Electrical Contacts to One- and Two-dimensional Nanomaterials. *Nat. Nanotechnol.* **2011**, *6*, 773−783.

(25) Kang, J.; Liu, W.; Sarkar, D.; Jena, D.; Banerjee, K. Computational Study of Metal Contacts to Monolayer Transition-metal Dichalcogenide Semiconductors. *Phys. Rev. X* **2014**, *4*, 031005.

(26) Zhong, H.; Quhe, R.; Wang, Y.; Ni, Z.; Ye, M.; Song, Z.; Pan, Y.; Yang, J.; Yang, L.; Lei, M.; et al. Interfacial Properties of Monolayer and Bilayer MoS_2 Contacts with Metals: Beyond the Energy Band Calculations. *Sci. Rep.* **2016**, *6*, 21786.

DOI: 10.1021/acs.jpcc.6b02696
J. Phys. Chem. C 2016, 120, 13063−13070

(27) Wang, Y.; Yang, R. X.; Quhe, R.; Zhong, H.; Cong, L.; Ye, M.; Ni, Z.; Song, Z.; Yang, J.-B.; Shi, J.-j.; et al. Does P-type Ohmic Contact Exist in WSe_2-metal Interfaces? *Nanoscale* **2016**, *8*, 1179−91.
(28) Gong, C.; Colombo, L.; Wallace, R. M.; Cho, K. The Unusual Mechanism of Partial Fermi Level Pinning at Metal-MoS_2 Interfaces. *Nano Lett.* **2014**, *14*, 1714−1720.
(29) Kang, J.; Liu, W.; Banerjee, K. High-performance MoS_2 Transistors with Low-resistance Molybdenum Contacts. *Appl. Phys. Lett.* **2014**, *104*, 093106.
(30) Chen, W.; Santos, E. J.; Zhu, W.; Kaxiras, E.; Zhang, Z. Tuning the Electronic and Chemical Properties of Monolayer MoS_2 Adsorbed on Transition Metal Substrates. *Nano Lett.* **2013**, *13*, 509−514.
(31) Çakır, D.; Peeters, F. M. Dependence of the electronic and transport properties of metal-$MoSe_2$ interfaces on contact structures. *Phys. Rev. B: Condens. Matter Mater. Phys.* **2014**, *89*, 245403.
(32) Zheng, J.; Wang, Y.; Wang, L.; Quhe, R.; Ni, Z.; Mei, W. N.; Gao, Z.; Yu, D.; Shi, J.; Lu, J. Interfacial Properties of Bilayer and Trilayer Graphene on Metal Substrates. *Sci. Rep.* **2013**, *3*, 2081.
(33) Giovannetti, G.; Khomyakov, P.; Brocks, G.; Karpan, V.; van den Brink, J.; Kelly, P. Doping Graphene with Metal Contacts. *Phys. Rev. Lett.* **2008**, *101*, 026803.
(34) Castro Neto, A. H.; Guinea, F.; Peres, N. M. R.; Novoselov, K. S.; Geim, A. K. The Electronic Properties of Graphene. *Rev. Mod. Phys.* **2009**, *81*, 109−162.
(35) Morales, J.; Santos, J.; Tirado, J. L. Electrochemical Studies of Lithium and Sodium Intercalation in $MoSe_2$. *Solid State Ionics* **1996**, *83*, 57−64.
(36) Kresse, G.; Joubert, D. From Ultrasoft Pseudopotentials to the Projector Augmented-wave Method. *Phys. Rev. B: Condens. Matter Mater. Phys.* **1999**, *59*, 1758−1775.
(37) Perdew, J. P.; Burke, K.; Ernzerhof, M. Generalized Gradient Approximation Made Simple. *Phys. Rev. Lett.* **1996**, *77*, 3865−3868.
(38) Perdew, J. P.; Wang, Y. Accurate and Simple Analytic Representation of the Electron-gas Correlation Energy. *Phys. Rev. B: Condens. Matter Mater. Phys.* **1992**, *45*, 13244−13249.
(39) Monkhorst, H. J.; Pack, J. D. Special Points for Brillouin-zone Integrations. *Phys. Rev. B* **1976**, *13*, 5188−5192.
(40) Smith, D. R.; Schultz, S.; Markoš, P.; Soukoulis, C. M. Determination of Effective Permittivity and Permeability of Metamaterials from Reflection and Transmission Coefficients. *Phys. Rev. B: Condens. Matter Mater. Phys.* **2002**, *65*, 195104.
(41) Soler, J. M.; Artacho, E.; Gale, J. D.; García, A.; Junquera, J.; Ordejón, P.; Sanchez-Portal, D. The SIESTA Method for Ab Initio Order-N Materials Simulation. *J. Phys.: Condens. Matter* **2002**, *14*, 2745−2779.
(42) *ATOMISTIX Toolkit*, version 11.8; QuantumWise A/S: Copenhagen, Denmark, 2011.
(43) Ma, Y.; Dai, Y.; Guo, M.; Niu, C.; Lu, J.; Huang, B. Electronic and Magnetic Properties of Perfect, Vacancy-doped, and Nonmetal Adsorbed $MoSe_2$, $MoTe_2$ and WS_2 Monolayers. *Phys. Chem. Chem. Phys.* **2011**, *13*, 15546−15553.
(44) Pan, Y.; Wang, Y.; Wang, L.; Zhong, H.; Quhe, R.; Ni, Z.; Ye, M.; Mei, W. N.; Shi, J.; Guo, W.; et al. Graphdiyne-metal Contacts and Graphdiyne Transistors. *Nanoscale* **2015**, *7*, 2116−2127.
(45) Jiang, H. Electronic Band Structures of Molybdenum and Tungsten Dichalcogenides by the *GW* Approach. *J. Phys. Chem. C* **2012**, *116*, 7664−7671.
(46) Pan, Y.; Wang, Y.; Ye, M.; Quhe, R.; Zhong, H.; Song, Z.; Peng, X.; Yu, D.; Yang, J.; Shi, J.; et al. Monolayer Phosphorene−Metal Contacts. *Chem. Mater.* **2016**, *28*, 2100−2109.
(47) Das, S.; Zhang, W.; Demarteau, M.; Hoffmann, A.; Dubey, M.; Roelofs, A. Tunable Transport Gap in Phosphorene. *Nano Lett.* **2014**, *14*, 5733−5739.
(48) Das, S.; Chen, H. Y.; Penumatcha, A. V.; Appenzeller, J. High Performance Multilayer MoS_2 Transistors with Scandium Contacts. *Nano Lett.* **2013**, *13*, 100−105.
(49) Liu, H.; Neal, A. T.; Zhu, Z.; Luo, Z.; Xu, X.; Tománek, D.; Ye, P. D. Phosphorene: an Unexplored 2D Semiconductor with a High Hole Mobility. *ACS Nano* **2014**, *8*, 4033−4041.

DOI: 10.1021/acs.jpcc.6b02696
J. Phys. Chem. C 2016, 120, 13063−13070